

Hoyle band and α condensation in ^{12}C

Y. Funaki*

Nishina Center for Accelerator-Based Science, Institute of Physical and Chemical Research (RIKEN), Wako 351-0198, Japan

(Received 25 August 2014; revised manuscript received 26 June 2015; published 3 August 2015)

The excited states in ^{12}C are investigated by using an extended version of the so-called Tohsaki-Horiuchi-Schuck-Röpke (THSR) wave function, where both the 3α condensate and $^8\text{Be} + \alpha$ cluster asymptotic configurations are included. A new method is also used to resolve spurious continuum coupling with physical states. I focus on the structures of the “Hoyle band” states (0_2^+ , 2_2^+ , and 4_2^+), which were recently observed above the Hoyle state, and of the 0_3^+ and 0_4^+ states, which were also quite recently identified in experiment. Their resonance parameters and decay properties are reasonably reproduced. All these states have dilute density structure of the 3α or $^8\text{Be} + \alpha$ clusters with larger root mean square radii than that of the Hoyle state. The Hoyle band is not simply considered to be the $^8\text{Be}(0^+) + \alpha$ rotation as suggested by previous cluster model calculations, nor to be a rotation of a rigid-body triangle-shaped object composed of the 3α particles. This is mainly due to the specificity of the Hoyle state, which has the 3α condensate structure and gives rise to the 0_3^+ state with a prominent $^8\text{Be}(0^+) + \alpha$ structure as a result of very strong monopole excitation from the Hoyle state.

DOI: [10.1103/PhysRevC.92.021302](https://doi.org/10.1103/PhysRevC.92.021302)

PACS number(s): 21.60.Gx

Nuclear clustering is one of the fundamental degrees of freedom in nuclear excitation [1]. The Hoyle state, the second $J^\pi = 0^+$ state at 7.654 MeV in ^{12}C , as a typical example of the cluster states, has a long history ever since it was predicted by Hoyle [2] and subsequently observed by Cook *et al.* [3] as a key state in the synthesis of ^{12}C in stellar evolution. The microscopic and semimicroscopic cluster models have clarified that the Hoyle state has the structure of the α particle loosely coupling in an S wave with the $^8\text{Be}(0^+)$ core [4–7], not like a linear-chain structure of the 3α particles proposed by Morinaga in the 1950’s [8]. In the last decade, however, the aspect of the α condensate, where the 3α clusters occupy an identical S orbit, has triggered great interest, since the so-called Tohsaki-Horiuchi-Schuck-Röpke (THSR) wave function [9], which has the α condensate character, was shown to be equivalent to the Hoyle state wave function obtained by solving the equations of the full 3α resonating group method (RGM) or generator coordinate method (GCM) [10].

On the other hand, the excited states of the Hoyle state have been highlighted by recent great developments in experimental studies. The second 2^+ state (2_2^+), which had been predicted at a few MeV above the Hoyle state by the cluster model calculations [5,6], was recently confirmed by many experiments [11–16]. The GCM and RGM calculations propose that the 2_2^+ state is built on the Hoyle state as a rotational member with a $^8\text{Be}(0^+) + \alpha$ configuration. Freer *et al.* quite recently reported a new observation of the 4^+ state at 13.3 MeV, which they consider to compose the “Hoyle band” [17], together with the 0_2^+ and 2_2^+ states. It is proposed that this band is formed by a rotation of a rigid 3α cluster structure with an equilateral triangle shape based on D_{3h} symmetry [18,19], which is, however, not consistent with the picture of loosely coupled $^8\text{Be}(0^+) + \alpha$ structure or the 3α gaslike structure.

Besides the 2^+ and 4^+ states, a 0^+ state at 10.3 MeV with a broad width, $\Gamma \approx 3$ MeV, has been known for a long time.

However, quite recently Itoh *et al.* decomposed the broad 0^+ state into the 0_3^+ and 0_4^+ states at 9.04 and 10.56 MeV, with the widths of 1.45 and 1.42 MeV, respectively [13]. This observation of the two 0^+ states is consistent with theoretical prediction done by using the orthogonality condition model (OCM) combined with the complex scaling method (CSM) and the analytical continuation of coupling constant (ACCC) method [20]. This was later confirmed by another theoretical calculation using the OCM and CSM with higher numerical accuracy [21].

On the other hand, in the antisymmetrized molecular dynamics (AMD) [22], fermionic molecular dynamics (FMD) [23], and GCM calculations [6], the observed 0_3^+ state seems to be missing. The 0_3^+ state given by the AMD and FMD, which may correspond to the observed 0_4^+ state, is dominated by a linear-chain-like configuration of the 3α clusters and is not inconsistent with the 0_3^+ state obtained by the GCM calculation [6], or with the 0_4^+ state in Ref. [20], where [$^8\text{Be}(2^+) \otimes l = 2$] $_0$ configuration is dominant. It should also be mentioned that the authors in Ref. [20] claimed that the 0_3^+ state has an S -wave dominant structure with more dilute density than that of the Hoyle state. These are also consistent with the observed decay properties of the 0_3^+ and 0_4^+ states that the former only decays into the [$^8\text{Be}(0^+) \otimes l = 0$] $_0$ channel and the latter decays into the [$^8\text{Be}(2^+) \otimes l = 2$] $_0$ channel with a sizable partial α -decay width [24].

In this Rapid Communication, I investigate the structures of the positive parity excited states above the 3α threshold by using an extended version of the THSR wave function [25] so as to include $^8\text{Be} + \alpha$ asymptotic configurations with a treatment of resonances. In particular, I focus on the “Hoyle band” (the 0_2^+ , 2_2^+ , and 4_2^+ states¹), and the 0_3^+ and 0_4^+ states, together with the corresponding experimental data, though I also obtained some other positive parity excited states.

¹I hereafter mention the 4^+ state at 13.3 MeV as the 4_2^+ state, for simplicity, though it is located lower than the 4^+ state at 14.08 MeV which forms the ground-state rotational band.

*funaki@riken.jp

The extended version of the THSR wave function is written as follows:

$$\Phi_{JM}^{\text{THSR}}(\mathbf{B}_1, \mathbf{B}_2) = \widehat{P}_{MK}^J \mathcal{A} \left[\exp \left\{ - \sum_{i=1}^2 \mu_i \sum_{k=x,y,z} \frac{\xi_{ix}^2}{B_{ik}^2} \right\} \phi^3(\alpha) \right], \quad (1)$$

where the $\phi(\alpha)$ is an intrinsic wave function of the α particle, and where the $(0s)^4$ configuration of the four nucleons is assumed with the size parameter b , which is kept fixed at $b = 1.348$ fm as almost the same value as at free space. ξ_i is the Jacobi coordinates between the 3α particles and $\mu_i = i/(i+1)$, for $i = 1, 2$. This is a fully microscopic wave function and every nucleons are antisymmetrized by \mathcal{A} . \widehat{P}_{MK}^J is an angular-momentum-projection operator, acting on the intrinsic state featured by the deformed Gaussian orbits and giving the total angular momentum J , in which the relative angular-momentum channels $[{}^8\text{Be}(I) \otimes I]_J$ are implicitly included. The parameters \mathbf{B}_1 and \mathbf{B}_2 in this wave function correspond to the sizes of the ${}^8\text{Be}$ core and the remaining α particle center-of-mass (c.m.) motion, respectively. In the subsequent calculations, the axial symmetric deformation is assumed, i.e., $\mathbf{B}_i = (B_{ix} = B_{iy}, B_{iz})$ ($i = 1, 2$), for simplicity. One should note that the case of $\mathbf{B}_1 = \mathbf{B}_2$ results in the original THSR wave function, where the c.m. motions of the 3α particles relative to the total c.m. position are condensed into a lowest energy $0S$ orbit, reflecting the bosonic feature [26,27]. While the original THSR wave function has a product form of the three α -particle wave functions, this new THSR wave function is a natural extension of the original version, since its basic concept is kept as a product form of the 2α (${}^8\text{Be}$)- and the α -cluster wave functions, where the 2α particles and the remaining α particle are allowed to occupy different orbits. Taking $|\mathbf{B}_1| \ll |\mathbf{B}_2|$ thus corresponds to the ${}^8\text{Be} + \alpha$ cluster gas, deviating from the identical 3α cluster gas for $b \ll \mathbf{B}_1 = \mathbf{B}_2$. It should also be mentioned that the THSR-type wave functions were recently shown to give the best description for various cluster states such as the ${}^{16}\text{O} + \alpha$ inversion doublet band in ${}^{20}\text{Ne}$ [28], 3α - and 4α -linear-chain states [29], and $2\alpha + \Lambda$ cluster states in ${}^9\text{Be}$ [30].

For the excited states above the 3α threshold, it is well known that the application of the bound state approximation gives accidental mixing between spurious continuum states and resonances. By using the fact that the root mean square (rms) radii of spurious continuum states are calculated to be extremely large within the bound state approximation, I developed a new method to extricate the mixing between the resonances and continuum states and to remove the spurious continuum components [31]. First I diagonalize the operator of mean square radius as follows:

$$\sum_{\mathbf{B}'_1, \mathbf{B}'_2} \left[\langle \Phi_{JM}^{\text{THSR}}(\mathbf{B}_1, \mathbf{B}_2) | \frac{1}{12} \sum_{i=1}^{12} (\mathbf{r}_i - \mathbf{X}_G)^2 | \Phi_{JM}^{\text{THSR}}(\mathbf{B}'_1, \mathbf{B}'_2) \rangle - \{R^{(\gamma)}\}^2 \langle \Phi_{JM}^{\text{THSR}}(\mathbf{B}_1, \mathbf{B}_2) | \Phi_{JM}^{\text{THSR}}(\mathbf{B}'_1, \mathbf{B}'_2) \rangle \right] g^{(\gamma)}(\mathbf{B}'_1, \mathbf{B}'_2) = 0, \quad (2)$$

where \mathbf{X}_G is the total c.m. position. I then remove out of the present model space the eigenstates belonging to unphysically large eigenvalues. By taking the following bases,

$$\Phi_{JM}^{(\gamma)} = \sum_{\mathbf{B}_1, \mathbf{B}_2} g^{(\gamma)}(\mathbf{B}_1, \mathbf{B}_2) \Phi_{JM}^{\text{THSR}}(\mathbf{B}_1, \mathbf{B}_2), \quad (3)$$

with γ satisfying $R^{(\gamma)} \leq R_{\text{cut}}$, I diagonalize the Hamiltonian as follows:

$$\sum_{\gamma'} \langle \Phi_{JM}^{(\gamma)} | H | \Phi_{JM}^{(\gamma')} \rangle f_{\lambda}^{(\gamma')} = E_{\lambda} f_{\lambda}^{(\gamma)}. \quad (4)$$

For the Hamiltonian, I adopt Volkov No. 2 force [32], with the strength parameters slightly modified [33], as an effective nucleon-nucleon interaction. For diagonalizing the operator of the rms radius in Eq. (2), I adopt 8^4 mesh points for the four-parameter set, $B_{1x} = B_{1y}, B_{1z}, B_{2x} = B_{2y}, B_{2z}$, up to around 80 fm. Since the present extended THSR wave function can include the ${}^8\text{Be} + \alpha$ asymptotic form by taking the large values of the two width parameters \mathbf{B}_1 and \mathbf{B}_2 , the ${}^8\text{Be} + \alpha$ continuum components, as well as the 3α continuum components, can be successfully removed by imposing the cutoff for the mean square radius $R^{(\gamma)} \leq R_{\text{cut}}$. More details will be shown in a forthcoming full paper.

Although I could not obtain the excited states except for the 0_2^+ and 2_2^+ states by using the original THSR wave function [26], one can now obtain the other observed 0_3^+ , 0_4^+ , and 4_2^+ states by using the present extended THSR wave function with a treatment of resonances. Since all these states are resonances above the 3α threshold, one then calculates the partial widths of the α particle decaying into $[{}^8\text{Be}(I) \otimes I]_J$ channel, which I simply denote as $[I, I]_J$, based on the R -matrix theory [34], with the following relations:

$$\Gamma_{[I, I]_J} = 2P_l(ka) \gamma_{[I, I]_J}^2, \quad \gamma_{[I, I]_J}^2 = \frac{\hbar^2}{2\mu a} |a \mathcal{Y}_{[I, I]_J}(a)|^2, \quad (5)$$

where $P_l(ka)$ is the penetrability calculated from the Coulomb wave functions, and k , a , and μ are the wave numbers of the relative motion, channel radius, and reduced mass, respectively. $\mathcal{Y}_{[I, I]_J}(r)$ is the α reduced width amplitude (RWA) defined as

$$\mathcal{Y}_{[I, I]_J}(r) = \sqrt{\frac{12!}{4!8!}} \langle [\Phi_I({}^8\text{Be}), Y_I(\hat{\xi}_2)]_{JM} \frac{\delta(\xi_2 - r)}{\xi_2^2} \phi(\alpha) | \Psi_{JM}^{(\lambda)} \rangle, \quad (6)$$

TABLE I. Dependence of the energy and rms radius on the cutoff parameter R_{cut} for the 0_2^+ , 0_3^+ , and 0_4^+ states.

R_c	0_2^+		0_3^+		0_4^+	
	$E - E_{3\alpha}^{\text{theor}}$	R_{rms}	$E - E_{3\alpha}^{\text{theor}}$	R_{rms}	$E - E_{3\alpha}^{\text{theor}}$	R_{rms}
5.2	0.39	3.5	4.6	4.0	4.3	3.5
5.6	0.31	3.6	3.7	4.2	4.4	3.8
6.0	0.23	3.7	2.6	4.7	3.9	4.2
6.4	0.22	3.8	2.4	4.8	3.9	4.2
6.8	0.22	3.8	2.4	4.9	3.9	4.3

TABLE II. Calculated binding energies (MeV) measured from the 3α threshold, $E - E_{3\alpha}^{\text{theor}}$, rms radii (fm) for mass distributions, R_{rms} , partial α -decay widths (MeV) into $^8\text{Be}(0^+)$ and $^8\text{Be}(2^+)$ channels, $\Gamma_{\text{calc}}(^8\text{Be} : 0^+) = \Gamma_{[0,J]J}$, $\Gamma_{\text{calc}}(^8\text{Be} : 2^+) = \sum_J \Gamma_{[2,J]J}$ in Eq. (5), and total width (MeV), $\Gamma_{\text{calc}}(\text{total}) = \Gamma_{\text{calc}}(^8\text{Be} : 0^+) + \Gamma_{\text{calc}}(^8\text{Be} : 2^+)$. The corresponding experimental data, which are taken from Ref. [13] for the 0_3^+ , 0_4^+ , and 2_2^+ states and from Ref. [17] for the 4_2^+ state, are also shown. The adopted channel radii a (fm) are shown in parentheses. The observed energies are input in the calculations of the penetration factor $P_l(ka)$ in Eq. (5). The cutoff parameter value $R_{\text{cut}} = 6.0$ fm is adopted.

States	$E - E_{3\alpha}^{\text{theor}}$	R_{rms}	$\Gamma_{\text{calc}}(^8\text{Be} : 0^+)$	$\Gamma_{\text{calc}}(^8\text{Be} : 2^+)$	$\Gamma_{\text{calc}}(\text{total})$	Expt.	
						$E - E_{3\alpha}^{\text{theor}}$	Γ_{expt}
0_2^+	0.23	3.7	2.5×10^{-6} ($a = 4.5$) 7.6×10^{-6} ($a = 5.5$)		2.5×10^{-6} 7.6×10^{-6}	0.3794	$8.5(10) \times 10^{-6}$
0_3^+	2.6	4.7	1.1 ($a = 9.0$) 0.94 ($a = 10.0$)		1.1 0.9	1.77(9)	1.45(18)
0_4^+	3.9	4.2	0.57 ($a = 4.0$) 0.53 ($a = 4.5$)	1.3×10^{-2} ($a = 6.0$) 2.6×10^{-2} ($a = 7.0$)	0.58 0.55	3.29(6)	1.42(8)
2_2^+	1.6	3.9	0.69 ($a = 5.5$) 0.93 ($a = 6.5$)	$< 10^{-6}$	0.69 0.93	2.57(6)	1.01(15)
4_2^+	3.7	4.5	1.7 ($a = 8.5$) 1.1 ($a = 10.0$)	1.1 ($a = 7.0$) 0.85 ($a = 8.0$)	2.8 2.0	6.0(2)	1.7(2)

where $\Psi_{JM}^{(\lambda)}$ is the eigenfunction in Eq. (4), $\Psi_{JM}^{(\lambda)} = \sum_{\gamma} f_{\lambda}^{(\gamma)} \Phi_{JM}^{(\gamma)}$.

Table I shows the energy and rms radii dependence on the parameter R_{cut} for the 0^+ states. Although for $R_{\text{cut}} < 6.0$ fm, even the Hoyle state energy is not converged well, and accordingly the higher 0_3^+ and 0_4^+ states do not have stable values of the energies and rms radii. However, if one takes $R_{\text{cut}} \geq 6.0$ fm, the results get rather stable for all the states. On the other hand, one should avoid taking larger values, in this case, more than $R_{\text{cut}} = 7.0$ fm, since it is found by using a pseudopotential method explained in Ref. [31] that spurious continuum states are again getting mixed with the resonances. This tendency is also the same for the 2_2^+ and 4_2^+ states.

The binding energies, which are measured from the 3α threshold, and α -decay widths of the five states are displayed in Table II in comparison with the corresponding experimental data. For the 0_3^+ and 0_4^+ states, the calculated energies are slightly higher than those of the observed 0_3^+ and 0_4^+ states, respectively. However, the calculated α -decay width of the 0_3^+ state, $\Gamma = 1.1$ MeV ($a = 9.0$ fm), is in good agreement with the observed width $\Gamma = 1.45$ MeV. For the 0_4^+ state, the decay energy into the $^8\text{Be}(2^+) + \alpha$ channel is very small. Therefore the partial width of this decay channel is very sensitive to the energy position. In Ref. [24], the authors reported a new peak at 10.8 MeV for the 0_4^+ state, which decays into the $^8\text{Be}(2^+) + \alpha$ channel with a partial width of 0.4 MeV. If one adopts this energy for calculating the width of the 0_4^+ state, the partial

decay width is as high as 0.12 MeV, which is comparable to the experimental data. For the 2_2^+ and 4_2^+ states, the calculated energies and widths are in reasonable agreement with the corresponding experimental data. In particular, the α -decay widths of about 1 MeV for the 2_2^+ state and about 2 MeV for the 4_2^+ state are reasonably reproduced by this calculation. Furthermore, the R_{cut} dependence of the widths is rather weak and the uncertainty by the variation of the adopted proper values is within about 10 %.

In Table II, I also show the rms radii of the five states. The rms radius of the Hoyle state, $R_{\text{rms}} = 3.7$ fm, is the smallest, which still corresponds to very low density, i.e., $(3.7/2.4)^3 = 3.7$ times lower than that of the ground state. The 0_3^+ , 0_4^+ , 2_2^+ , and 4_2^+ states have 7.5, 5.4, 4.3, and 6.6 times lower densities than that of the ground state, respectively. This means that all these states have loosely coupled structures of the 3α or $^8\text{Be} + \alpha$ clusters, which are quite different from the rigid-body localized structure of the 3α clusters. Next I discuss the nature of the Hoyle band. Table III shows the $E2$ transition strengths and monopole matrix elements, with uncertainties coming from the cutoff dependence. Very strong $E2$ transitions can be seen between the 4_2^+ and 2_2^+ states, and between the 2_2^+ and 0_2^+ states. The transitions between the 2_2^+ and 0_3^+ states and between the 2_2^+ and 0_4^+ states are about two times and ten times weaker than the one between the 2_2^+ and 0_2^+ states, respectively. This allows one to consider that the 0_2^+ , 2_2^+ , and 4_2^+ states form a rotational band, though the strength between

TABLE III. Calculated $E2$ transition strengths $B(E2)$ and monopole matrix elements $M(E0)$ in units of $e^2 \text{fm}^4$ and fm^2 , respectively, with uncertainty from the variation of the adopted cutoff values, ranging from 6.0 to 6.8 fm for the 0^+ states and from 6.0 to 6.4 fm for the 2_2^+ and 4_2^+ states. The observed data are also shown for the $B(E2)$ and $M(E0)$ in the right column.

	Calc.		Calc.	Expt.
$B(E2; 2_2^+ \rightarrow 0_2^+)$	295-340	$B(E2; 2_1^+ \rightarrow 0_1^+)$	9.5	7.6(4)
$B(E2; 4_2^+ \rightarrow 2_2^+)$	560-730	$B(E2; 2_1^+ \rightarrow 0_2^+)$	1.0	2.6(4)
$B(E2; 2_2^+ \rightarrow 0_3^+)$	88-220	$B(E2; 2_2^+ \rightarrow 0_1^+)$	2.0-2.5	0.73(13)
$B(E2; 2_2^+ \rightarrow 0_4^+)$	22-31	$M(E0; 0_2^+ \rightarrow 0_1^+)$	6.3-6.4	5.4(2)
$M(E0; 0_2^+ \rightarrow 0_3^+)$	34-37			
$M(E0; 0_2^+ \rightarrow 0_4^+)$	0.5-1.4			

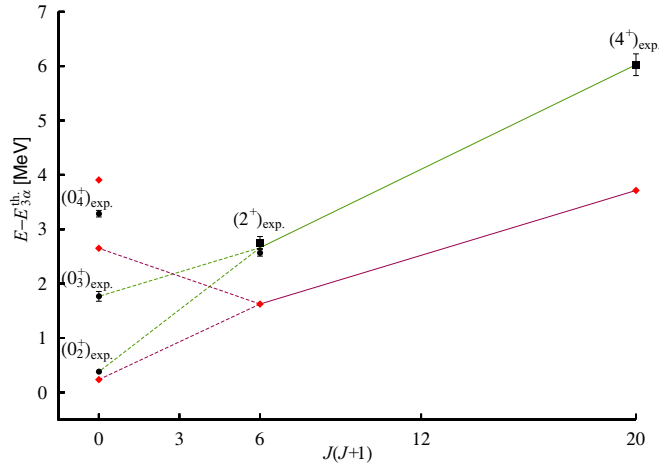


FIG. 1. (Color online) Observed energy levels for the 0_3^+ , 0_4^+ , and 2_2^+ states in Ref. [13], and the 2_2^+ [16] and 4_2^+ [17] states are denoted by black circles and black squares, respectively. The calculated energy levels for the five states are denoted by red diamonds. The cutoff parameter value $R_{\text{cut}} = 6.0$ fm is adopted.

the 2_2^+ and 0_3^+ states is still large enough, so that the 0_3^+ state may influence the band nature.

In Fig. 1, the calculated energy levels are plotted as a function of $J(J+1)$, together with the corresponding experimental data. The 0_2^+ , 2_2^+ , and 4_2^+ states both in theory and experiment roughly follow a $J(J+1)$ trajectory. However, the $J^\pi = 0^+$ bandhead in experiment seems to be fragmented into the Hoyle state and the 0_3^+ state, and the calculated levels also have a similar tendency, where the Hoyle state is located slightly below the $J(J+1)$ line. This indicates that this Hoyle band is not a simple rotational band.

Figure 2 shows the calculated S^2 factors of the $\alpha + {}^8\text{Be}$ components, which can be defined as

$$S_{[I,I]}^2(J_\lambda^+) = \int dr [r \mathcal{Y}_{[I,I]}(r)]^2. \quad (7)$$

One can see that except for the 0_4^+ state, all the states have the largest contribution from the $[0, J]_J$ channel. This supports the idea of ${}^8\text{Be} + \alpha$ rotation for the Hoyle band, where the ${}^8\text{Be}$ core is in the 0^+ ground state and is consistent with the previous GCM calculation [6]. The 0_3^+ state in the GCM calculation may correspond to my 0_4^+ state since both states dominantly have the $[2, 2]_0$ component, while my 0_3^+ state may be missing in the GCM calculation.

On the other hand, the Hoyle state is considered to be the 3α condensate state, where the 3α clusters mutually move in an identical S wave. Since the ground state of ${}^8\text{Be}$ is composed of weakly interacting 2α clusters coupled loosely in a relative S wave, it is natural that the Hoyle state, with the α condensate structure, also has a large overlap with the ${}^8\text{Be}(0^+) + \alpha$ structure. This is the same situation as for the 4α condensate state in ${}^{16}\text{O}$ discussed in Refs. [35,36], which has a large overlap with the ${}^{12}\text{C}(0_2^+) + \alpha$ structure.

However, the 3α condensate structure in the Hoyle state is not the same as ordinary ${}^8\text{Be}(0^+) + \alpha$ rotation, in which the remaining α cluster orbits outside the ${}^8\text{Be}$ core. Namely in the Hoyle state, the remaining α cluster also orbits inside the ${}^8\text{Be}$

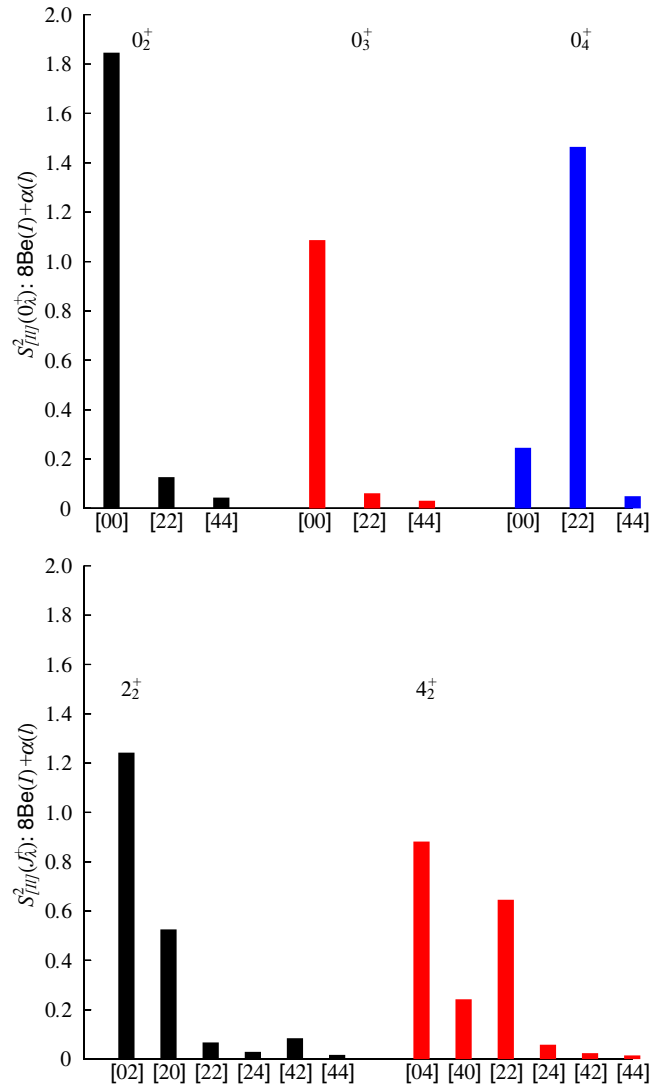


FIG. 2. (Color online) S^2 factors $S_{[I,I]}^2(J_\lambda^+)$ defined in Eq. (7) for the five J^π states. The cutoff parameter value $R_{\text{cut}} = 6.0$ fm is adopted.

core, and the independent 3α -cluster motion in an identical $0S$ orbit is realized. As a result, the Hoyle state gains an extra binding, and hence its energy position is considered to be made lower than the $J(J+1)$ line, as shown in Fig. 1. The same effect is also argued in the study of the 4α condensate and ${}^{12}\text{C}(0_2^+) + \alpha$ rotational band [37,38], where the 4α condensate is mentioned as “complete condensate” and the ${}^{12}\text{C}(0_2^+) + \alpha$ state as “local condensate.” Due to the existence of the complete condensate, a higher 0^+ excited state, which has the prominent ${}^8\text{Be}(0^+) + \alpha$ structure, with the remaining α cluster orbiting outside the ${}^8\text{Be}$ core, appears as a higher nodal state, that is the 0_3^+ state. In fact, one can see in Table III that the 0_3^+ state is strongly connected with the Hoyle state by a monopole excitation. The calculated strength $M(E0; 0_2^+ \rightarrow 0_3^+) \sim 35 \text{ fm}^2$ is much larger than the other transitions, in spite of the fact that the $E0$ strength between the Hoyle and ground states $M(E0; 0_2^+ \rightarrow 0_1^+) = 6.4 \text{ fm}^2$ is still strong enough as to be comparable to the single nucleon strength [39].

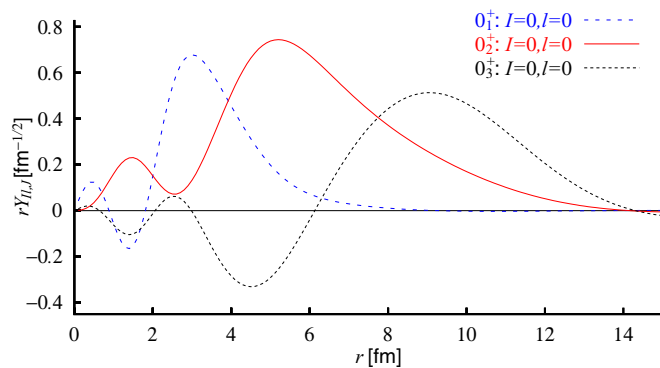


FIG. 3. (Color online) RWAs of the $[I, I]_J = [0, 0]_0$ channel, $Y_{[0,0]_0}(r)$ in Eq. (6), for the 0_1^+ , 0_2^+ , and 0_3^+ states. The cutoff parameter value $R_{\text{cut}} = 6.0$ fm is adopted.

In Fig. 3, the RWAs of $[0, 0]_0$ channel for the 0_2^+ and 0_3^+ states are shown together with that for the ground state. While the RWA for the ground state has two nodes, that for the 0_3^+ state has four nodes, and for the Hoyle state the nodal behavior almost disappears and only a remnant of three nodes can be seen as an oscillatory behavior. Since the outmost nodal position corresponds to a radius of repulsive core between the core ^8Be and the α cluster, due to the effect of the Pauli principle, the disappearance of the nodes for the Hoyle state indicates a dissolution of the ^8Be core, and hence formation of the 3α condensate. On the other hand, the 0_3^+ state, which is excited from the Hoyle state by the monopole transition, recovers the distinct nodal behavior and, with one additional node, forms a higher nodal $^8\text{Be}(0^+) + \alpha$ structure. This is consistent with the argument in Ref. [20], as mentioned in the Introduction.

In Fig. 2, the 0_4^+ state is shown to have the component of $[2, 2]_0$ channel dominantly, which gives rise to non-negligible partial decay width into this channel, consistently with the experimental information, as mentioned above. I also mention that the 2_2^+ state also includes a non-negligible mixture from the $[2, 0]_2$ channel and 4_2^+ states from the $[2, 2]_4$ channel and a smaller amount from the $[4, 0]_4$ channel. These mixtures also deviate the 2_2^+ and 4_2^+ states from a pure $^8\text{Be} + \alpha$ rotational structure. This tendency is not changed qualitatively by adopting the other proper cutoff parameter values.

In conclusion, the use of the extended THSR wave function allows one to obtain the wave functions of the Hoyle band and 0_3^+ and 0_4^+ states, which were recently confirmed by experiments. The calculated α -decay widths and the decay properties of these states are in good agreement with the experimental data. All these states are shown to have large rms radii and hence dilute density 3α or $^8\text{Be} + \alpha$ cluster structures. The 0_2^+ , 2_2^+ , and 4_2^+ states are not considered to form a simple $^8\text{Be}(0^+) + \alpha$ rotational band, due to the specificity of the Hoyle state with the 3α condensate feature, which allows the 0_3^+ state to have a prominent $^8\text{Be}(0^+) + \alpha$ structure as a result of the strong monopole excitation.

The author expresses special thanks to H. Horiuchi and A. Tohsaki for their valuable and helpful discussion and suggestions on the present work. The fruitful discussion with M. Itoh is highly appreciated. Thanks are also due to G. Röpke, P. Schuck, T. Yamada, and B. Zhou for their stimulating discussion. This work was partially performed with the financial support by HPCI Strategic Program of Japanese MEXT, JSPS KAKENHI Grant No. 25400288, and RIKEN Incentive Research Projects.

-
- [1] K. Wildermuth and Y. C. Tang, *A Unified Theory of the Nucleus* (Vieweg, Braunschweig, 1977).
- [2] F. Hoyle, *Astrophys. J. Suppl. Ser.* **1**, 121 (1954).
- [3] C. W. Cook *et al.*, *Phys. Rev.* **107**, 508 (1957).
- [4] H. Horiuchi, *Prog. Theor. Phys.* **51**, 1266 (1974); **53**, 447 (1975).
- [5] Y. Fukushima *et al.*, *Suppl. J. Phys. Soc. Jpn.* **44**, 225 (1978); M. Kamimura, *Nucl. Phys. A* **351**, 456 (1981).
- [6] E. Uegaki, S. Okabe, Y. Abe, and H. Tanaka, *Prog. Theor. Phys.* **57**, 1262 (1977); E. Uegaki, Y. Abe, S. Okabe, and H. Tanaka, *ibid.* **62**, 1621 (1979).
- [7] P. Descouvemont and D. Baye, *Phys. Rev. C* **36**, 54 (1987).
- [8] H. Morinaga, *Phys. Rev.* **101**, 254 (1956); *Phys. Lett.* **21**, 78 (1966).
- [9] A. Tohsaki, H. Horiuchi, P. Schuck, and G. Röpke, *Phys. Rev. Lett.* **87**, 192501 (2001).
- [10] Y. Funaki, A. Tohsaki, H. Horiuchi, P. Schuck, and G. Röpke, *Phys. Rev. C* **67**, 051306(R) (2003).
- [11] M. Itoh *et al.*, *Nucl. Phys. A* **738**, 268 (2004).
- [12] M. Freer *et al.*, *Phys. Rev. C* **80**, 041303(R) (2009).
- [13] M. Itoh *et al.*, *Phys. Rev. C* **84**, 054308 (2011).
- [14] H. O. U. Fynbo and M. Freer, *Physics* **4**, 94 (2011).
- [15] W. R. Zimmerman, N. E. Destefano, M. Freer, M. Gai, and F. D. Smit, *Phys. Rev. C* **84**, 027304 (2011).
- [16] W. R. Zimmerman *et al.*, *Phys. Rev. Lett.* **110**, 152502 (2013).
- [17] M. Freer *et al.*, *Phys. Rev. C* **83**, 034314 (2011).
- [18] R. Bijker and F. Iachello, *Phys. Rev. C* **61**, 067305 (2000); *Ann. Phys. (Amsterdam)* **298**, 334 (2002).
- [19] D. J. Marín-Lámbarri, R. Bijker, M. Freer, M. Gai, Tz. Kokalova, D. J. Parker, and C. Wheldon, *Phys. Rev. Lett.* **113**, 012502 (2014).
- [20] C. Kurokawa and K. Kato, *Phys. Rev. C* **71**, 021301 (2005); *Nucl. Phys. A* **792**, 87 (2007).
- [21] S.-I. Ohtsubo, Y. Fukushima, M. Kamimura, and E. Hiyama, *Prog. Theor. Exp. Phys.* (2013) 073D02.
- [22] Y. Kanada-En'yo, *Prog. Theor. Phys.* **117**, 655 (2007).
- [23] M. Chernykh, H. Feldmeier, T. Neff, P. von Neumann-Cosel, and A. Richter, *Phys. Rev. Lett.* **98**, 032501 (2007).
- [24] M. Itoh *et al.*, *J. Phys.: Conf. Ser.* **436**, 012006 (2013).
- [25] B. Zhou, Y. Funaki, A. Tohsaki, H. Horiuchi, and Z. Z. Ren, *Prog. Theor. Exp. Phys.* (2014) 101D01.
- [26] Y. Funaki, A. Tohsaki, H. Horiuchi, P. Schuck, and G. Röpke, *Eur. Phys. J. A* **24**, 321 (2005).
- [27] Y. Funaki, H. Horiuchi, W. von Oertzen, G. Röpke, P. Schuck, A. Tohsaki, and T. Yamada, *Phys. Rev. C* **80**, 064326 (2009).
- [28] B. Zhou, Y. Funaki, H. Horiuchi, Z. Z. Ren, G. Röpke, P. Schuck, A. Tohsaki, C. Xu, and T. Yamada, *Phys. Rev. Lett.* **110**, 262501 (2013).

- [29] T. Suhara, Y. Funaki, B. Zhou, H. Horiuchi, and A. Tohsaki, *Phys. Rev. Lett.* **112**, 062501 (2014).
- [30] Y. Funaki, T. Yamada, E. Hiyama, B. Zhou, and K. Ikeda, *Prog. Theor. Exp. Phys.* (2014) 113D01.
- [31] Y. Funaki, H. Horiuchi, and A. Tohsaki, *Prog. Theor. Phys.* **115**, 115 (2006).
- [32] A. B. Volkov, *Nucl. Phys. A* **74**, 33 (1965).
- [33] Y. Fujiwara, H. Horiuchi, K. Ikeda, M. Kamimura, K. Katō, Y. Suzuki, and E. Uegaki, *Suppl. Prog. Theor. Phys.* **68**, 29 (1980).
- [34] A. M. Lane and R. G. Thomas, *Rev. Mod. Phys.* **30**, 257 (1958).
- [35] Y. Funaki, T. Yamada, H. Horiuchi, G. Röpke, P. Schuck, and A. Tohsaki, *Phys. Rev. Lett.* **101**, 082502 (2008).
- [36] Y. Kanada-En'yo, *Phys. Rev. C* **89**, 024302 (2014).
- [37] S. Ohkubo and Y. Hirabayashi, *Phys. Lett. B* **684**, 127 (2010).
- [38] Y. Funaki, T. Yamada, H. Horiuchi, G. Röpke, P. Schuck, and A. Tohsaki, *Suppl. Prog. Theor. Phys.* **196**, 439 (2012).
- [39] T. Yamada, Y. Funaki, H. Horiuchi, K. Ikeda, and A. Tohsaki, *Prog. Theor. Phys.* **120**, 1139 (2008).